Toward a synthesis of equatorial spread *F* onset and suppression during geomagnetic storms

C. R. Martinis, M. J. Mendillo, and J. Aarons
Center for Space Physics, Boston University, Boston, Massachusetts, USA

Received 20 December 2003; revised 7 March 2005; accepted 24 March 2005; published 22 July 2005.

[1] We present initial steps toward unifying our understanding of storm time equatorial spread *F* (ESF) by searching for the common elements in past case studies and statistical occurrence patterns. We show that the development (or inhibition) of equatorial irregularities during magnetically active periods can be understood using the *AE*-parameterized Fejer-Scherliess model for disturbance vertical drifts versus storm time and local time. This model takes into account the different sources of perturbation electric fields (magnetospheric and ionospheric dynamos) that ultimately drive the equatorial vertical drifts, showing prompt and delayed effects in the premidnight sector (where both generation and suppression can occur), as well as in the postmidnight period where generation dominates. The postsunset period exhibits the greatest variability for storm time ESF versus longitude, and thus we demonstrate the Fejer-Scherliess model's applicability in a test case (6 April 2000) that had an *AE* pattern compatible with their parameterization scheme. The model successfully accounts for the pronounced longitude confinement in the observed postsunset ESF patterns. Finally, we move beyond the empirically derived relationships between geomagnetic indices and the occurrence of ESF (Aarons, 1991) into a framework of true solar-terrestrial parameters that drive such effects. Additional case studies taken from the published literature are then used to show a consistent linkage between postsunset ESF onset and the interplanetary electric field (IEF) E_{sw}. While *AE*, *Dst*, *Kp* and *Dst*/*dt* indices were used in earlier studies to determine the dusk-longitude sector of disturbance electric fields, here we attribute to the IEF the main role in the determination of this longitude sector.

Citation: Martinis, C. R., M. J. Mendillo, and J. Aarons (2005), Toward a synthesis of equatorial spread *F* onset and suppression during geomagnetic storms, *J. Geophys. Res.*, *110*, A07306, doi:10.1029/2003JA010362.

1. Introduction

1.1. Climatology and Day-to-Day Variability of Equatorial Ionospheric Irregularities

[2] Geomagnetic storms can affect the dynamics of the low-latitude ionosphere in very significant ways. Global circulation models have made great progress dealing with geomagnetic effects on changes in neutral composition, neutral winds, electrodynamics, and their disturbances upon large-scale electron density morphologies [*Fuller-Rowell et al.*, 2002; *Richmond et al.*, 2003]. Simulation studies have not yet advanced to modeling small-scale irregularities during storms. This is due in part to the unclear message that has emerged from decades of observations that have not lead to a consistent net effect of geomagnetic activity on the triggering or inhibition of equatorial irregularities.

[3] The spectrum of small-scale equatorial irregularities collectively known as equatorial spread *F* (ESF) is generated by the gravitationally driven Rayleigh-Taylor instability. The growth rate γ_{RT} of this instability (neglecting chemical recombination) can be expressed as

$$\gamma_{RT} = \underset{(a)}{\frac{\Sigma_P^F}{\Sigma_P^E + \Sigma_P^F}} \underset{(b)}{\frac{\vec{\nabla} N}{N}} \cdot \left[\underset{(c)}{\frac{\vec{E} \times \vec{B}}{B^2}} - \underset{(d)}{\frac{\vec{g}}{\nu_{in}}} - \underset{(e)}{\vec{U}_n} \right] \tag{1}$$

[4] All the parameters in (1) are flux-tube integrated quantities [*Haerendel et al.*, 1992; *Sultan*, 1996]. If the growth rate is positive then the instability will develop. After a few $(\gamma_{RT})^{-1}$ timescales (tens of minutes to ~1 hour), irregularities are fully developed and can be detected with a variety of means (e.g., ionosondes, radars, satellites, all-sky imagers, satellite radio beacons). For ESF to develop, there are five processes that might be subdivided into two enabling conditions and three driving/suppressing effects represented in (1). The enabling effects occur after sunset, when the *F* region to total (*E* + *F*) region Pedersen conductivity ratio (***a***) approaches unity and the electron density gradient, $\nabla N/N$, (***b***) is large. Upward $\mathbf{E} \times \mathbf{B}$ drifts (***c***) have been observed to be the main drivers for the

0148-0227/05/2003JA010362$09.00

generation of ESF. It is generally accepted that a strong upward drift in the postsunset period is the single most important condition for ESF to occur [*Fejer et al.*, 1999; *Mendillo et al.*, 2001]. Enhancing effects occur when the ionosphere moves to high altitudes, reducing the collision frequency between ions and neutrals ν_{in} and thus causing (***d***) to be large. The neutral wind term (***e***) refers to the component perpendicular to the magnetic field. In the context of flux tube integrated analysis $U_n = U_m \sin I + U_v \cos I$, where U_m and U_v are the meridional and vertical components of the total wind in the geomagnetic meridian and I is the magnetic inclination angle. *Raghavarao et al.* [1993] discussed the role of vertical neutral winds over the magnetic equator, a region where the vertical component is assumed to be small compared with the meridional one. There is no conclusive observational evidence to support a role of day-to-day changes in meridional neutral winds upon ESF [*Mendillo et al.*, 2001], while simulations tend to include it as a suppressant for ESF.

[5] All of the general patterns for the occurrence of postsunset irregularities during quiet geomagnetic periods determined from diverse sets of observations can be understood using (1). A seasonal and longitudinal pattern of ESF occurrence has been described [*Aarons*, 1993; *Huang et al.*, 2001], generally consistent with the alignment of the sunset terminator with magnetic field declination, as proposed by *Tsunoda* [1985], and the effect of seasonal meridional winds [*Maruyama and Matuura*, 1984; *Maruyama*, 1988]. Thus the months of June and July show minimal occurrence of ESF in the South American sector: the disappearances of the *E* regions are not simultaneous at the two extremes of the field line, so γ_{RT} is reduced because the term (***a***) is small. Yet this is a season of high occurrence of ESF in the Pacific Sector, where the magnetic declination and sunset terminator angle is close to zero, allowing the conductivity ratio term to approach unity and pressure gradients along a geomagnetic meridian (and hence winds) to be minimal.

[6] While the monthly longitudinal behavior of ESF and its solar activity dependence can be explained in a satisfactory way, the day-to-day variability and geomagnetic storm effects are still issues not fully understood. It is not clear why during "ESF season" at a given longitude, irregularities occur only on certain days and not on every day. Past studies tried to understand this nonuniform occurrence pattern by examining the influence of day-to-day changes in single effects, e.g., meridional neutral winds [*Mendillo et al.*, 2001] or the presence of sporadic *E* [*Stephan et al.*, 2002]. In attempts to understand day-to-day variability in ESF, the role of vertical drifts continues to emerge as the consistent, required, and dominant agent for ESF occurrence. The key to understanding quiet time ESF may well be linked to understanding its storm time behavior, since potential source characteristics can be more reliably identified during dramatic disturbances.

1.2. Previous Studies of ESF and Geomagnetic Activity

[7] Attempts to find a correlation between geomagnetic activity and the occurrence of small-scale irregularities in the low-latitude ionosphere have produced a vast literature of apparently contradictory results. The early report by *Lyon et al.* [1960] suggested that ESF is inhibited during geomagnetic storms. Their study, based on ionosonde data taken during the International Geophysical Year (IGY), showed that the percentage of occurrence of ESF was drastically reduced during periods of geomagnetic activity.

[8] In the 1970s and 1980s, advancements were made as many authors were able to distinguish between the influence of storms on postsunset and postmidnight ESF. A general consensus emerged that postmidnight ESF tended to be triggered by storms [*Aarons et al.*, 1980; *Dabas et al.*, 1989]. Inhibition effects were reported during the postsunset period [*Alex and Rastogi*, 1986; *Dabas et al.*, 1989]. Other studies concluded that postsunset ESF was triggered during non-ESF season, while it was inhibited during ESF season [*Aarons et al.*, 1980; *Rastogi et al.*, 1981], a pattern recently confirmed by *Becker-Guedes et al.* [2004].

[9] Taken together, these studies show that geomagnetic storms can (1) either inhibit or trigger the occurrence of postsunset ESF and (2) trigger the occurrence of postmidnight ESF. Thus a clear and undisputed effect of geomagnetic storms is the generation of postmidnight ESF. For this situation, if one were to ignore local time (i.e., no distinction between postsunset and postmidnight) and ask the question "Do storms provoke ESF?" the answer would be yes. The answer to that question would not convey a clear message, however, if drawn from the reports on the geomagnetic activity influence on postsunset ESF.

[10] In the 1990s, a pivotal advance in ESF studies came from the work of *Aarons* [1991] that explored the presence or absence of irregularities versus longitude and storm time by considering the universal time of the storm's peak effect (in his case using $|Dst|$). Thus in *Abdu*'s [1997] study of the influence of disturbance winds and electric fields generated by geomagnetic storms on the equatorial ionization anomaly and ESF, he found that triggering or inhibition of ESF would occur depending on the phase of the storm. More recently, *Su. Basu et al.* [2001] related the occurrence of strong irregularities with rates of change of *Dst* larger than -50 nT/h. *Huang et al.* [2002] considered a less stringent criterion and concluded that rates of change larger than an arbitrarily chosen value of -5 nT/h for 2 or more hours would trigger equatorial irregularities, likely due to the penetration of high-latitude electric fields. *Sobral et al.* [2002] used the K_p index to show a correlation between large values in the 1900–2100 LT period and the occurrence of irregularities.

[11] Thus the concept introduced by *Aarons* [1991] has become the operative paradigm for current studies. This concept, now known as the "Aarons criteria" [*Biktash*, 2004], basically states that the use of a geomagnetic index to portray peak storm time can identify the longitude sector most susceptible to ESF onset. *Su. Basu et al.* [2001] used it to show that equatorial irregularities occur in the specific longitude sector for which the early evening period corresponds to the time of rapid *Dst* variation and strongly negative *Dst* values. *Biktash* [2004] used it to analyze five storm events and discussed how different indices characterize the "peak storm time." Thus in this paper we begin with the Aarons criteria as a validated basic premise (i.e., the use of a geomagnetic index to find the longitude sector susceptible to the occurrence of ESF) and explore how solar-terrestrial coupling processes can account for such correlations.

[12] The studies presented above considered vertical drifts as the key parameter to determine the occurrence of

ESF. In the equatorial region, vertical plasma drifts are produced by zonal electric fields. Typically, daytime (nighttime) electric fields are eastward (westward) and produce upward (downward) drifts. The decay of the *E* region after sunset produces an enhancement in the upward drifts prior to its change to downward motion. This feature, called the prereversal enhancement, has been explained by different theories [*Farley et al.*, 1986; *Haerendel and Eccles*, 1992] and simulated successfully in general circulation models [*Fesen et al.*, 2000]. A clear relation exists between the magnitude of the prereversal enhancement and occurrence of postsunset ESF: irregularities are more likely to develop when a strong prereversal enhancement is present. The strength will depend on the prevailing geophysical conditions, e.g., at solar maximum, a threshold level of ~50 m/s is required, while during solar minimum it is reduced to ~20 m/s [*Fejer et al.*, 1999].

[13] Thus because upward $\mathbf{E} \times \mathbf{B}$ drifts are the main drivers for the generation of ESF, understanding geomagnetic storm effects on ESF requires understanding storm time $\mathbf{E} \times \mathbf{B}$ drifts at the equator. This brings us to the electrodynamical mechanisms that are not generated locally but rather ones that reach low latitudes from distant sources.

1.3. Magnetospheric and Ionospheric Dynamos

[14] Low-latitude electric fields can be significantly disturbed during storms and other magnetically active conditions. Two major sources of these perturbations are found in the magnetospheric and ionospheric disturbance dynamos. Magnetospheric dynamo processes generate short-lived (termed "prompt") electric field perturbations with time scales less than ~2 hours, depending on magnetospheric plasma properties and ionospheric conductivity [*Jaggi and Wolf*, 1973; *Southwood and Wolf*, 1978; *Siscoe*, 1982; *Senior and Blanc*, 1984]. The driver of the magnetospheric dynamo can be found in the solar wind. The magnetospheric dynamo converts solar wind energy into electromagnetic energy in the magnetosphere via reconnection processes between the solar wind and Earth's magnetic fields. The nature of this interaction depends strongly on the direction of the interplanetary magnetic field (IMF). The magnetosphere intercepts, on average, 10–20% of the solar wind voltage that would occur across its diameter. This magnetospheric potential is then impressed onto the ionosphere, where it becomes the high-latitude polar cap potential Φ_{pc} that generates field aligned Region 1 currents (the higher-latitude current system in the auroral region). Early studies correlated Φ_{pc} with combinations of various solar wind parameters, especially the speed v_{sw} and the IMF southward component B_z [*Reiff and Luhmann*, 1986; *Boyle et al.*, 1997; *Burke et al.*, 1999]. Prompt penetration of electric fields is caused by rapid changes in Φ_{pc} that produce sudden Region 1 current variations. Region 2 currents (the lower-latitude current system in the auroral region) cannot change at the same rate and an imbalance situation occurs. Thus the high-latitude electric potential pattern, usually circumscribed to this region under quiet conditions by Region 2 currents, can reach much lower latitudes. The so-called shielding is broken and electric fields can be observed at low latitudes. Specifically, for sudden increases in Φ_{pc}, the situation is called undershielding. On the other hand, when Φ_{pc} suddenly decreases, Region 2 currents remain large and electric fields of opposite polarity can propagate to lower latitudes (overshielding condition). Thus the polar cap potential behavior is key to understanding how prompt penetration effects occur.

[15] The ionospheric disturbance dynamo, on the other hand, results from thermospheric disturbance winds generated by Joule heating at auroral latitudes during periods of high magnetic activity [*Blanc and Richmond*, 1980; *Richmond et al.*, 2003]. These disturbance winds affect the low-latitude region several hours after the increase in magnetic activity. These winds are equatorward of Region 2 currents and any electric fields they generate are not shielded from the low-latitude ionosphere. They produce changes in the ionospheric dynamo (long-lived effects) that are more persistent than those associated with the magnetospheric dynamo (prompt effects). In this study we will focus on how these cases relate to ESF, with specific attention to the prompt effects due to the magnetospheric dynamo.

2. Storm Time ESF

2.1. An Empirical Vertical Drift Model

[16] Equatorial vertical plasma drifts obtained from incoherent scatter radar measurements at the Jicamarca Radio Observatory were used by *Scherliess and Fejer* [1997] and *Fejer and Scherliess* [1997] to study the storm time dependence of electric field disturbances due to ionospheric and magnetospheric dynamos. They determined the perturbation drifts by subtracting seasonal and solar cycle effects. These perturbed drifts were then ordered as a function of the *AE* index, a parameter related to the polar cap potential drop [*Ahn et al.*, 1992], and the energy input in the high-latitude ionosphere [*Ahn et al.*, 1983]. Owing to their different timescales, the low-latitude effects of both processes can be separated and the relation between local time and storm time can be explored. Figure 1, adapted from *Fejer* [2002], shows an idealized change in the *AE* index, representing the polar cap potential Φ_{pc}, and the response of the disturbance equatorial vertical drifts for different storm times. Individual points in the plot are determined by binning the data, and the solid curves are obtained from the analytical model. The scatter bars denote the standard deviations of the individual points. The magnitudes of the disturbance drifts are small because they average many different storm scenarios. Thus the important information in Figure 1 is the characteristic pattern of storm time disturbance drifts at different local times and not necessarily their average magnitudes.

[17] For a sudden increase in the *AE* index (or Φ_{pc}), high-latitude electric fields penetrate almost instantaneously to the low-latitude ionosphere [*Kikuchi et al.*, 2000]. These prompt penetration electric fields are eastward during the day and westward at night [*Nopper and Carovillano*, 1978] producing perturbed upward and downward drifts, respectively. Storm times t_0 and t_1 can be related to prompt penetration timescales. During these storm times, then, the implications are that ESF could be triggered at postsunset (and inhibited during the postmidnight period, although ESF is not generated after midnight during quiet conditions).

[18] Prompt penetration effects are short-lived, however, and thus after a few hours disturbance dynamo effects start to control the dynamics of the low-latitude region. At storm

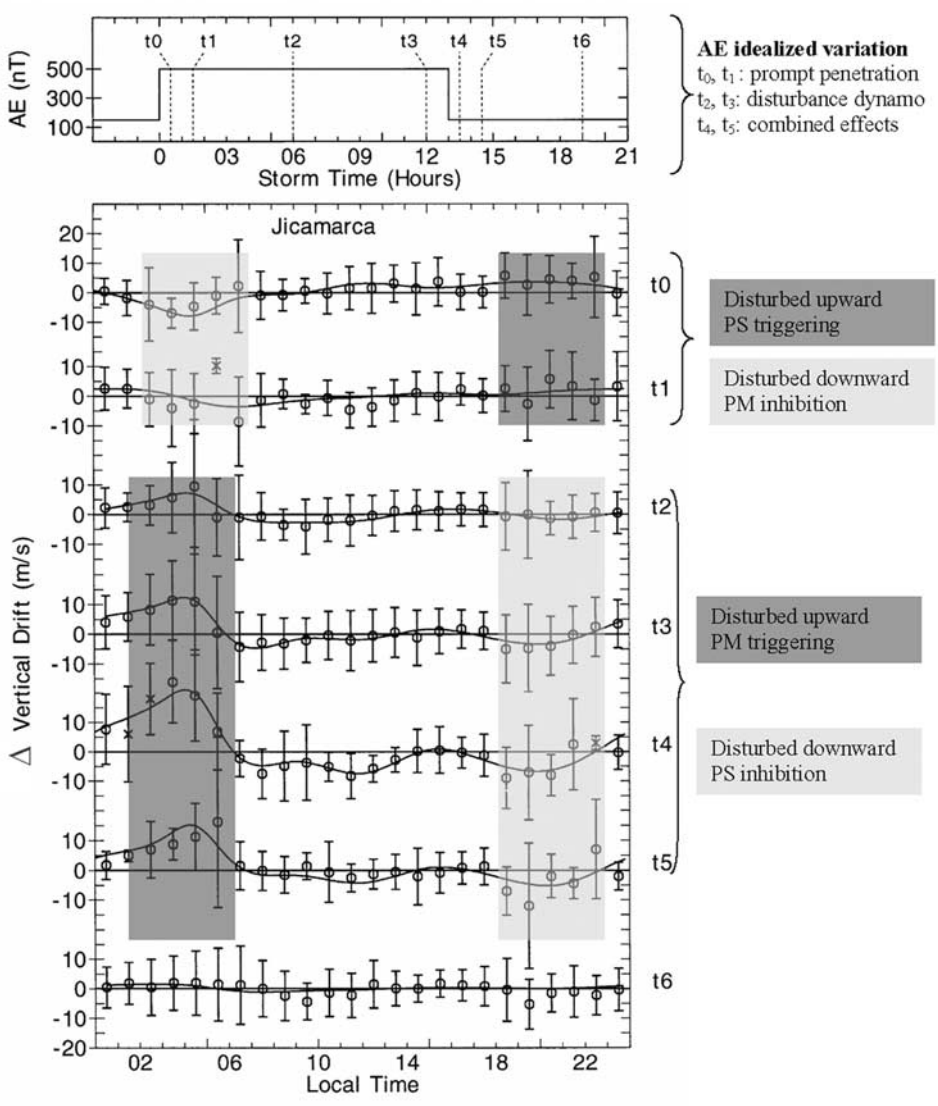

Figure 1. Local time variation of perturbed vertical drifts in the equatorial ionosphere due to prompt penetration electric fields and disturbance dynamo effects. Circles indicate Jicamarca observations with scatter bars representing standard deviations. Solid curves indicate model results. Light (dark) shaded boxes have been added to emphasize periods with downward (upward) perturbed drifts that contribute to inhibition (generation) of ESF; PS = postsunset and PM = postmidnight. (Adapted from *Fejer* [2002]).

times t_2 and t_3, the only effects are those caused by the disturbance dynamo that produces upward and downward disturbance drifts during the night and day, respectively. Note that the duration of the penetration times (t_0 and t_1) and the isolation of the disturbance dynamo (t_2 and t_3) depend fundamentally on the parameterization scheme that characterizes the transition from uniform-quiet to uniform-disturbed via a simple step function.

[19] The sudden decrease in *AE* following t_3 produces an overshielding situation and again a prompt penetration electric field can reach low latitudes. Now, both dynamos add to produce the largest perturbations in the vertical drifts at storm time t_4, downward for most of the day, but upward from midnight to dawn. Postsunset ESF would thus be inhibited, while the large disturbance upward vertical drift would contribute to the generation of postmidnight ESF. At t_5 the disturbance dynamo is still effective, while the prompt penetration effects have vanished, prolonging postsunset inhibition and postmidnight generation of irregularities. Finally, at t_6, disturbance drifts are not observed.

[20] Figure 1 offers a framework for a unified understanding of storm time ESF. In particular, it provides the context that explains the history of different accounts (generation versus inhibition) for the geomagnetic activity effects upon ESF. We can relate upward (downward) disturbance vertical drifts with the generation (inhibition) of irregularities. A problem arises in moving forward with this concept due to the fact that all of the statistical and case studies mentioned earlier use *Dst* or K_p, while *AE* was used

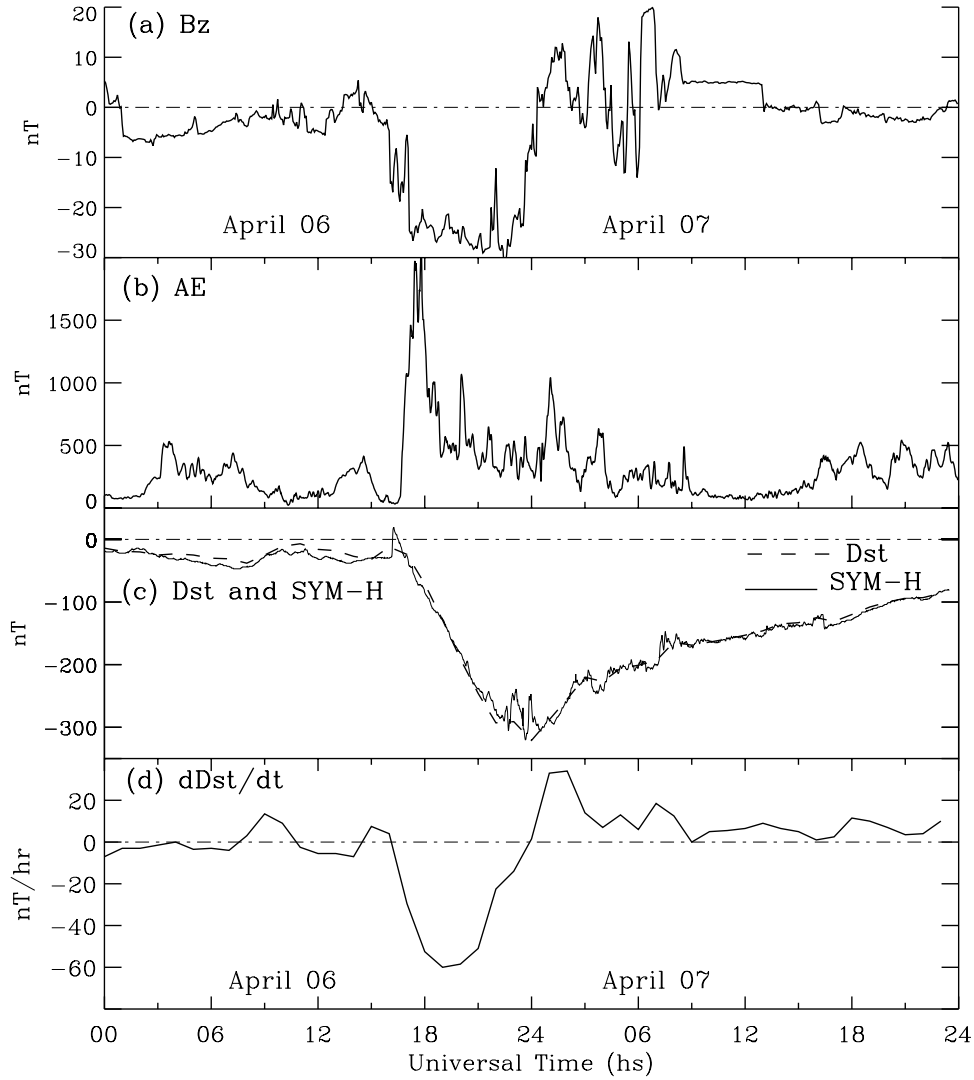

Figure 2. Example of a geomagnetic storm (6–7 April 2000) with a sudden onset in *AE* compatible with the storm time vertical plasma drift model. (a) Interplanetary magnetic field B_z measured by ACE; (b) *AE* index; (c) equatorial *Dst* (dashed) and SYM-H (solid line) indices; (d) rate of change of *Dst* index.

to order the key physical process (vertical drift) that drives ESF. Moreover, the use of *AE* to parameterize prompt effects can sometimes be misleading (i.e., it can underestimate the real value of Φ_{pc}, especially when the auroral oval is equatorward of the stations used to measure *AE*). Nevertheless, it has been a key tool to understand the climatology of disturbance vertical drifts in the equatorial ionosphere, and thus we proceed using it for storm scenarios, leaving its relationship to physical drivers for section 3.

2.2. The 6 April 2000 Magnetic Storm

[21] Figure 1 employs an idealized storm pattern in *AE* to order superposed-epoch effects. We now use the 6 April 2000 storm as one that approaches the empirical vertical drift model's parameterization, especially the abrupt increase in *AE* after quiet conditions. Figure 2 shows geophysical parameters and magnetic indices for the storm. Advanced Composition Explorer (ACE) observations of the IMF B_z show a strong southward component of ~ -25 nT after 1700 UT (the time delay to the magnetopause is $\sim$50 min). The auroral *AE* index reaches a maximum of 2000 nT near 1800 UT and the equatorial *Dst* index reaches a minimum value of ~ -300 nT at 2400 UT, but its rate of change is maximum between 1800 and 2100 UT. The abrupt increase in *AE* approaches the idealized behavior shown in the upper part of Figure 1. We will focus on the possible effects in the occurrence of ESF due to this sudden increase.

[22] Defense Meteorological Satellite Program (DMSP) satellite data are used to obtain ion densities in the low-latitude region. DMSP satellites are in circular, Sun-synchronous polar orbits near 840 km. The orbital planes for the satellites used (satellites F12 and F14) are near the 0930–2130 LT meridians. A good longitudinal coverage for the postsunset period was obtained by combining different satellite passes. Figure 3 shows the occurrence of irregularities only in the East African sector ($\sim$10°E to 35°E) during the 1818–2040 UT period. Thus postsunset irregularities occur while the geomagnetic storm is going through its main phase following the classic "longitudinally confined" scenario for storms embodied in the Aarons Criteria.

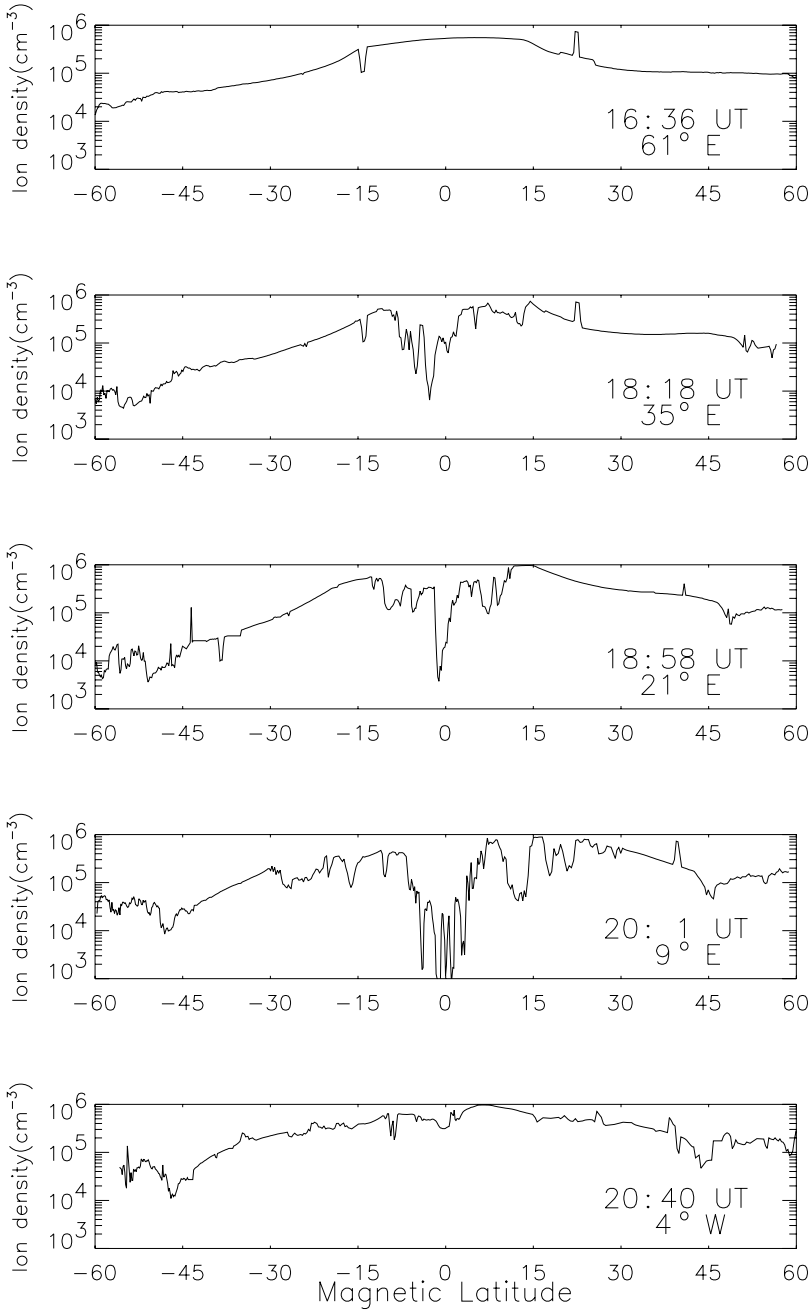

Figure 3. Ion densities from DMSP passes on 6 April 2000 at different longitudes from ~1636 UT to 2040 UT. Notice the occurrence of postsunset irregularities in the 9°E–35°E sector (East-African sector).

[23] Data from the International GPS Service for Geodynamics (IGS) can be processed to obtain phase fluctuations or rate of change of total electron content (TEC), a measure of the presence of ionospheric irregularities [*Mendillo et al.*, 2000]. GPS data can be obtained for an entire day for practically all longitudes, complementing the single meridian (two LT) coverage from DMSP satellites. Figure 4 shows phase fluctuation data for the only station with some activity during this period: Malindi (3°S, 40°E, −11.5° mag lat). Other low-latitude stations located at different longitudes (Kouru, Arequipa, Easter Island, Guam, and Diego Garcia) showed no irregularities during this period, demonstrating the highly localized occurrence of irregularities. Thus for most of the globe, postsunset ESF did not occur on this storm day.

[24] Taken together, Figures 3 and 4 (and all the GPS sites without TEC fluctuations) offer convincing evidence that the only sector showing irregularities was the relatively narrow longitude region between about 10°E and 40°E. If we identify 1800 UT as the t_0 storm time, the postsunset period (1900–2000 LT) corresponds to the 15°E to 30°E longitudinal sector. We can expect disturbance upward vertical drifts due to prompt penetration effects. To verify this, we run the Fejer-Scherliess empirical vertical drift model at 15° and 30°E, using as inputs a 15-min average *AE* and the corresponding *F*10.7 index. The results in

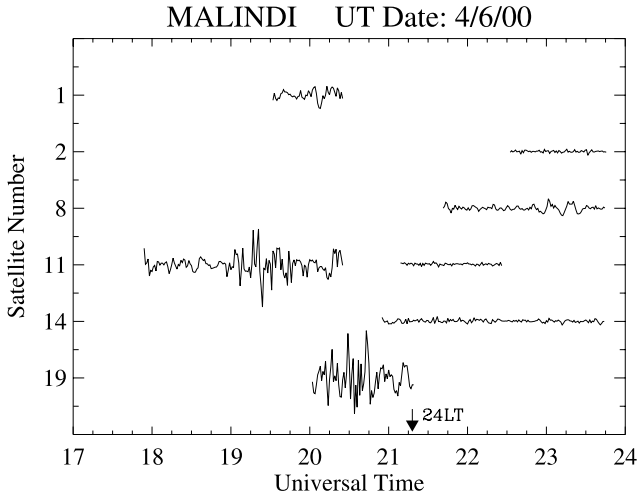

Figure 4. GPS phase fluctuations (expressed in units of total electron content, TECu, per minute) on 6 April 2000 observed at Malindi (40°E). Vertical axis represents satellite number. Separation between satellites is 2 TECU/min. GPS data from all other longitude sectors did not show irregularities in the post-sunset period. The vertical arrow indicates local midnight.

Figure 5 show the quiet vertical drifts and the disturbance vertical drifts due to prompt penetration effects. At 1800 UT the magnitude of the disturbance drift is 20 m/s. At 15°E, the prereversal enhancement increases from 40 m/s to approximately 60 m/s. At 30°E the disturbance drifts reduce the rapid downward motion of the ionosphere after sunset, and thus at 1800 UT the total drifts are ~0 m/s instead of −30 m/s. The third panel shows the drifts at 75°W. This longitude corresponds to one of the DMSP satellite passes that does not show the presence of irregularities. The disturbance drifts do not affect the postsunset period and thus storm time induced irregularities do not occur. These results explain the observations of irregularities in the 10°E to 40°E longitudinal sector: upward perturbed drifts help to create the right conditions for irregularities to develop only in the UT-determined longitude sector close to postsunset.

[25] To verify that upward plasma drifts did in fact occur, we examined data from a digisonde at Grahamstown in the same longitude sector (33°S, 26.5°E, −40° mag lat) and found that the virtual height of the bottomside *F* layer (h′*F*) goes from 220 km at 1900 UT to 470 km 2100 UT during 6 April. We associate the derived vertical drift of ~35 m/s with a strong perturbation electric field in this longitude sector that will contribute to the occurrence of ESF at low latitudes. Thus the results obtained from this individual case are consistent with the studies carried out by *Su. Basu et al.* [2001], *Huang et al.* [2002], and others who showed the occurrence of irregularities during the main phase of magnetic storms. In the next section we will show how several different cases can also be unified within the context of the Fejer-Scherliess model for the postsunset triggering of ESF.

2.3. Other Case Studies

[26] Several past studies have shown evidence of the occurrence of postsunset irregularities during geomagnetic storms. Particularly interesting were those reports of the occurrence of postsunset ESF during periods that normally would not lead to it (i.e., in the "non-ESF season" discussed earlier). In the Brazilian sector, June–July solstice is a period with very low occurrence of ESF. Nevertheless, *Sastri et al.* [1997] and *Sahai et al.* [1998, 2004] showed cases of postsunset ESF during this period when storms were in their main phase and *AE* indices were reaching their maximum values. Within the context of Figure 1 such events occurred at the parameterized times t_0 and t_1.

[27] Table 1 summarizes observational results found in the literature showing irregularities occurring in the postsunset period during large magnetic storms. The first four cases, showing a sudden increase in *AE*, can be unified by the use of Figure 1, i.e., according to the storm time t_o when penetration happened. For those cases not showing a sudden increase in *AE* (last three in Table 1) the proxy needed to determine t_o seems to be the rate of change of *Dst*. The Bastille Day storm, 15 July 2000, characterized by a steady increase in *AE* for ~10 hours until it reached its maximum at ~1900 UT, represents one of these cases. *Sa. Basu et al.* [2001] studied this storm and concluded that prompt penetration electric fields occurred between 1900 and 2100 UT and, as a consequence, postsunset ESF was generated at ~15°W. They determined this time by looking at the maximum rate of change of the SYM-H index (a 1-min equivalent of *Dst*). *Su. Basu et al.* [2001] analyzed two additional cases, 22 September 1999 and 22 October 1999, showing the influence of magnetic storms at middle and low latitudes. In both cases, the maximum rate of change of *Dst* served as a successful proxy for the time of prompt penetration. Yet, for these two cases, *AE* also showed a sudden increase at the same time the maximum *dDst*/*dt* is observed.

[28] In examining Table 1 further, one sees that the *AE* index cannot always be used to determine the time t_0 because it does not necessarily show abrupt changes (e.g., the 15 July 2000 storm). All the cases in Table 1 show that the rate of change of *Dst* is maximum when irregularities are observed in the corresponding postsunset longitude sector. We also include in Table 1 the values of B_z and interplanetary electric field (IEF) E_{sw} for that time. The common feature in all the cases is the presence of a large and consistent southward excursion in the IMF and large values of the IEF. This fact points clearly to the connection between solar wind drivers and their effects upon the equatorial ionosphere.

3. Discussion

3.1. ESF in the Context of the Fejer-Scherliess Model

[29] While ESF can (and does) occur throughout the night, in this study we focused primarily on the properties of the magnetic storm to trigger (or not inhibit) postsunset irregularities because this is the period of the most dramatic and severe ESF events. The mechanism involved is the prompt penetration of an eastward electric field that produces upward disturbance vertical drifts during the postsunset period. This extra push, besides affecting the latitudinal distribution of ionospheric plasma [*Valladares and Sheehan*, 2001], favors the conditions for the generation of equatorial irregularities. In the context of the Fejer-Scherliess empirical model, this corresponds to storm times t_0 and t_1, that is,

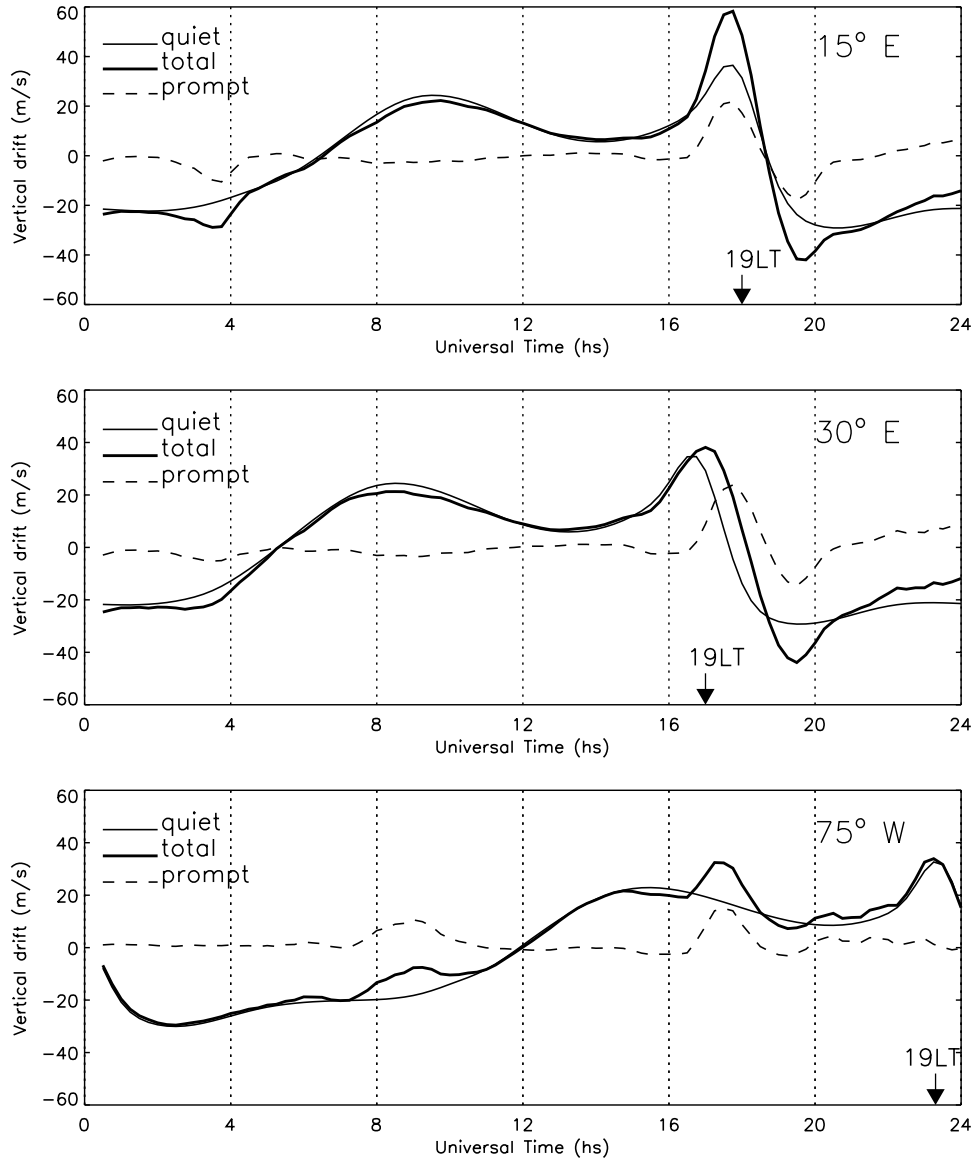

Figure 5. Calculated vertical drifts using the Fejer-Scherliess empirical model of vertical drifts [*Fejer*, 2002] and *AE* index (Figure 2b). Vertical drifts are shown at 15°E (top), 30°E (middle), and 75°W (bottom). The disturbance drifts due to prompt effects enhance the postsunset pattern of vertical drifts at 15° and 30°E, helping to create the right conditions for irregularities to develop. The bottom panel shows that the prompt disturbance drifts at 75°W occur earlier in local time and thus do not affect the postsunset period. Solid lines represent quiet condition vertical drifts; dashed lines indicate the contribution from prompt effects; thick lines indicate the resulting vertical drifts. Arrows indicate the typical time (1900 LT) of prereversal enhancement peak upward drifts.

Table 1. Storm Cases and Longitude Sectors Where ESF Occurs[a]

Storm	*AE*, nT	*dDst*/*dt*, nT/h	*Dst*, nT	B_z, nT	E_{sw}, mV/m	Longitude(s) of observed ESF	Reference
22 Oct 1999	1100 at 0100 UT*	−50 at 0100 UT	−250 at 0600 UT	−20 at 0000 UT	9 at 0000 UT	45°−190°W	*Su. Basu et al.* [2001]
	1300 at 0500 UT*	−55 at 0500 UT		−31 at 0500 UT	15 at 0500 UT		
6 April 2000	1400 at 1800 UT*	−60 at 1800−2100 UT	−300 at 2200 UT	−25 at 2100 UT	16 at 2100 UT	10°−50°E	This study
22 Sept 1999	900 at 2100 UT*	−70 at 2000−2200 UT	−180 at 2300 UT	−20 at 2100 UT	10 at 2200 UT	15°−75°W	*Su. Basu et al.* [2001]
4 June 1978	1000 at 2200 UT*	−15 at 2100−2200 UT	−70 at 0400 UT	−8 at 2200 UT	5 at 2200 UT	40°W	*Sastri et al.* [1997]
26 Aug 1998	1000 at 2200 UT†	−33 at 2300−0000 UT	−140 at 0300 UT	−11 at 0100 UT	8 at 0100 UT	40°W	*Sahai et al.* [2004]
18 July 1980	1100 at 2000 UT†	−35 at 2000−2200 UT	−80 at 2200 UT	−20 at 2100 UT	7 at 2100 UT	40°W	*Sastri et al.* [1997]
15 July 2000	1800 at 1800 UT†	−120 at 1900−2100 UT	−300 at 0000 UT	−60 at 2000 UT	40 at 2000 UT	15°W	*Sa. Basu et al.* [2001]

[a]For each storm case columns 2 to 6 represent the times in UT where the maximum values of the parameter occur. Values marked with an asterisk represent a sudden increase, while values marked with a cross represent a gradual increase.

after a sudden increase of the polar cap potential drop represented in the model by the *AE* index.

[30] The generation of postmidnight ESF is related to disturbance dynamo effects that produce perturbed upward drifts during this period. There is a vast published literature showing the occurrence of postmidnight ESF and it is accepted that disturbance dynamo effects are mainly responsible for the uplift that leads to the generation of ESF during this period. However, during postsunset, disturbance dynamo effects tend to inhibit the occurrence of ESF. Thus the empirical drift model can now be used to explain differing accounts of how magnetic storms affect ESF. Moreover, if one were to average the disturbance vertical drifts at a given local time, i.e., superpose the patterns of disturbance vertical drifts at the different storm times (from t_0 to t_6 in Figure 1), the average would show a net perturbed downward motion in the postsunset sector, resulting in an inhibition effect. A perturbed upward motion would occur in the postmidnight sector, creating the conditions to trigger ESF. These two independent and opposite motions clearly explain the conclusions reached in the early statistical studies of ESF and geomagnetic activity that did not take storm time into effect. Our extensive use of the Fejer-Scherliess model needs some qualifications. It is a climatological model, one that does not take into account some processes and parameters, e.g., the IMF B_y that might cause changes in the electric potential distribution and high-latitude energy deposition in different LT sectors that would affect the amplitude and local time distribution of the electric field perturbations [*Fejer and Scherliess*, 1997; *Fejer*, 2002].

3.2. Linkage Between Geomagnetic Indices and Solar Wind Parameters

[31] Four cases in Table 1 show that a sudden increase in *AE* is almost simultaneous with the maximum *dDst*/*dt*. Both *AE* and *dDst*/*dt* could be used as proxies to determine the time when penetration occurs. However, for the other three cases, *AE* does not present a sudden increase and it is the maximum *dDst*/*dt* that can be used to infer the penetration time. During the 15 July 2000 storm, for example, while AE started to increase several hours earlier, B_z showed a large southward component (or large E_{sw}) only after ~1900 UT. Owing to the steady (as opposed to sudden) increase in *AE*, the time t_0 cannot be determined by following the *AE* behavior. This case represents the situation when, trying to determine the time for prompt penetration, one index seems to be better than the other (*dDst*/*dt* instead of *AE*). We also indicate in Table 1 the time and magnitude of large and steady southward excursion of B_z, and, related to it, the maximum E_{sw}. A common pattern is observed in all cases: the presence of a strong and consistent southward B_z and a large E_{sw}.

[32] It should not be surprising that the use of different indices to portray the effects of magnetic storms on ESF give a similar answer. An increase in *AE* can be related, in general, to the main phase of a storm, when *Dst* is decreasing and its rate of change is largest. *Blanc* [1978], studying the midlatitude ionosphere, concluded that penetration effects could be due not to transient effects in the high-latitude region but to rapid changes in the ring current. They found that it happened when *dDst*/*dt* was ~−5 nT/h. *Su. Basu et al.* [2001] pointed out the importance of modeling prompt penetration electric fields as a function of the ring current. *Ridley and Liemohn* [2002] presented a model in which penetration of electric fields to midlatitudes happens when there is a divergence in the asymmetric ring current. They distinguish these electric fields from the penetration electric fields generated by insufficient shielding, obtaining an empirical relationship between the electric potential at low latitudes and *Dst** (the corrected *Dst* index, representing only the perturbations due to the ring current) and its rate of change *dDst**/*dt*. However, one of the boundary conditions in the model requires a zero potential at 35° magnetic latitude, so it is not yet possible to apply this model to the penetration potential near the magnetic equator.

[33] In Table 1 we showed that the determination of t_o was related to large *AE*, *dDst*/*dt*, and large southward excursion of B_z. Why should this be? In fact, many studies have tried to link the variations of these indices with variations in solar wind parameters [*Burton et al.*, 1975; *O'Brien and McPherron*, 2000; *Shen et al.*, 2002]. The basic assumption employed is that the rate of change of *Dst** is proportional to a ring current injection function, $Q(t)$, and the magnitude of the *Dst**, i.e.,

$$\frac{\mathrm{dDst^*}}{\mathrm{dt}} = \mathrm{Q(t)} - \frac{\mathrm{Dst^*}}{\tau} \tag{2}$$

where τ represents the ring current timescale for decay. *Burton et al.* [1975] considered a constant $\tau = 7.7$ hours and showed that $Q(t)$ is linearly proportional to the dawn-dusk solar wind electric field E_{sw}

$$\mathrm{Q(t)} = \begin{cases} 0 & \text{for } \mathrm{E_{sw}} < 0.5 \text{ mV/m} \\ -5.4(\mathrm{E_{sw}} - 0.5) & \text{for } \mathrm{E_{sw}} \geq 0.5 \text{ mV/m} \end{cases} \tag{3}$$

O'Brien and McPherron [2000] obtained a similar relation for $Q(t)$ with a decay time τ also a function of the dawn-dusk solar wind electric field. If $Q(t)$ is large (a large E_{sw}), the rate of change of *Dst** will also be large. If $Q(t)$ is equal to zero, *Dst** reached its minimum and it will recover exponentially with a time constant τ.

[34] There are expressions relating solar wind parameters and the polar cap potential [*Boyle et al.*, 1997; *Burke et al.*, 1999; *Siscoe et al.*, 2002] but none between polar cap potential and *Dst* or *dDst*/*dt*. If penetration occurs for *dDst*/*dt* larger than a certain threshold value, can this threshold for E_{sw} be calculated? Equations (2) and (3) should be useful to explore this possibility. Figure 6 shows how *Dst** and E_{sw} are related when different ring current rates and recover times are considered. For the 6 April 2000 storm, $dDst^*/dt = -60$ nT/h, $Dst^* \sim -250$ nT, and assuming τ equals 5 (or 10) hours, E_{sw} is about 15 (or 20) mV/m, close to the measured value (see Table 1). For the other cases in Table 1, where *Dst* and *Dst/dt* are used, the calculated values are also close to the measured ones. According to *Huang et al.* [2002], for $\mathrm{dDst^*}/dt \sim -5$ nT/h, equatorial irregularities were likely to develop. Using equation (3), depending on the strength of the storm, E_{sw} can vary from 5 to 10 mV/m. The important message we draw from these calculations

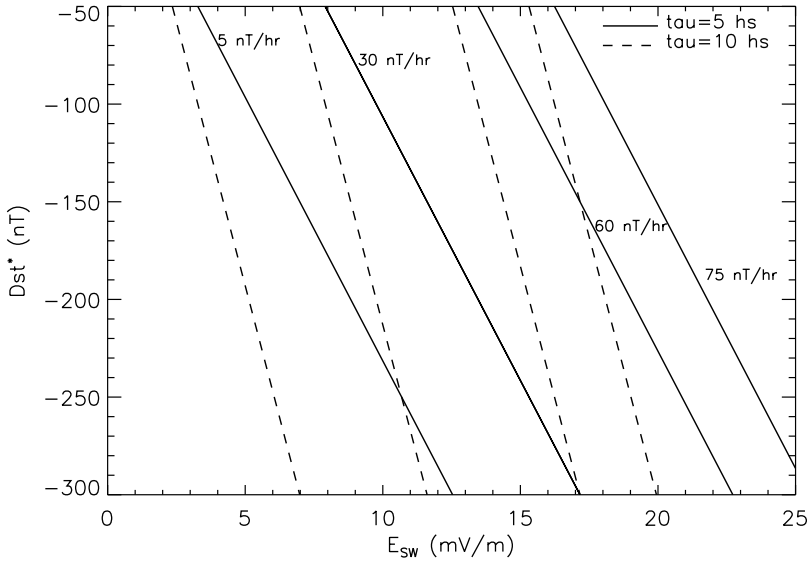

Figure 6. *Dst** and *dDst*/dt* relationship with the interplanetary electric field E_{sw}. Solid (dashed) lines are calculated with a recovery time τ of 5(10) hours for different *dDst*/dt* values. For the 6 April storm, with a *dDst*/dt* ~ -60 nT/h at *Dst** ≈ -250 nt, an E_{sw} between 16 and 21 mV/m is obtained.

is that while the rate of change values proposed span more than an order of magnitude (-5 nT/h and -60 nT/h), the corresponding E_{sw} values range from $\sim$5 to $\sim$15 mV/m, a much smaller range. Furthermore, with this simple calculation we can relate the behavior of a physical driver, in this case E_{sw}, to the occurrence of ESF.

[35] The suggestion of a link between equatorial electric fields and solar wind parameters was presented in the 1970s [*Rastogi and Patel*, 1975; *Fejer et al.*, 1979; *Kelley et al.*, 1979; *Gonzales et al.*, 1979]. For example, *Rastogi and Patel* [1975] studied the possible coupling between the equatorial ionosphere and the IMF. They concluded that large and rapid changes of the IMF from southward to northward direction can be associated with an electric field in the low-latitude ionosphere. *Fejer et al.* [1979] also explored the relation between the IMF B_z and the equatorial electric field but did not find conclusive evidence of a direct correlation. *Gonzales et al.* [1979] discussed the possible sources for disturbed equatorial electric fields; they involved direct penetration of high-latitude electric fields (like the ones in Fejer-Scherliess' work, prompt in nature) and field-aligned currents during asymmetric ring current events (like the ones in Ridley and Liemohn's work, with longer lifetime).

[36] Prompt penetration effects can also occur during the onset (sudden storm commencement, SSC) phase of magnetic storms. In this case, if we were to use a proxy, a positive *dDst*/*dt* should indicate the time for penetration. *Wilson et al.* [2001] show that after the SSC of the 8 July 1991 storm, DMSP satellites measured Φ_{pc} reaching values larger than 100 kV and equatorial irregularities were observed at $\sim$30°E, consistent with longitude-dusk UT effect (the SSC occurs at $\sim$1630 UT). They considered that a prompt penetration electric field due to the SSC reached the equatorial region and helped to trigger the irregularities. This inference was confirmed by *Sastri* [2002], who showed that within $\sim$1 hour of the SSC an eastward electric field disturbance occurred at the dusk-side magnetic equator.

[37] The study of direct penetration of the solar wind electric field E_{sw} into the equatorial region is a subject of renewed interest. For example, *Sazykin et al.* [2004] used idealized changes in solar wind parameters to calculate equatorial electric fields, considering changes in the polar cap potential, the reconfiguration of the magnetic field, and ring current properties. Also, *Rothwell et al.* [2004] merged the magnetospheric model of *Siscoe et al.* [2002] that relates the high-latitude polar cap potential with solar wind parameters and ionospheric conductance, with the global ionospheric potential model of *Nopper and Carovillano* [1978]. They calculated the equatorial electric fields generated by the magnetospheric dynamo. They considered a case with low solar activity and an IEF E_{sw} = 12 mV/m (similar conditions of the 6 April 2000 storm). The equatorial electric field calculated in the post-sunset sector was about 1 mV/m. This electric field would produce a vertical drift of $\sim$25 m/s. From Figure 5 we see that the Fejer-Scherliess prompt upward drift at 1900 LT is $\sim$20 m/s. Thus in the simple calculation presented here using equations (2) and (3), the range of E_{sw} between 5 and 15 mV/m seems to be a meaningful threshold value needed to trigger ESF.

[38] While we have offered a synthesis for the overall effects of magnetic storms on ESF and the importance of understanding prompt penetration electric fields for post-sunset generation, there are still unsolved issues that need to be addressed to understand the complex solar wind-magnetosphere-equatorial ionosphere coupling. For example, if penetration happens during the main phase of a storm, as seems to be more frequent, then a large E_{sw} is the main solar wind parameter needed to determine the longitude sector affected, while a large negative *dDst*/*dt* would be the proxy. However, if it happens during the SSC of certain storms, the main solar wind parameter is pressure, and the proxy needed is a positive *dDst*/*dt*. Both cases are related to

sudden changes in the behavior of solar wind parameters (a large southward excursion of IMF, the arrival of a pressure pulse in the magnetopause).

4. Conclusions

[39] We have reexamined a broad spectrum of issues related to the complex role of geomagnetic storms in the generation/inhibition of equatorial irregularities. For the postsunset period, day-to-day occurrence patterns for ESF are usually associated with the occurrence of upward plasma drifts in the *F* region. For storm periods, we used the Fejer-Scherliess empirical model that provides perturbed vertical drifts as a function of storm time, as parameterized by *AE*, to explain onset (or suppression). For the postsunset period, both generation and suppression of ESF can occur, depending on which dynamo (magnetospheric or ionospheric) is dominant. For the postmidnight period, when quiet time ESF does not usually occur, the ionospheric disturbance dynamo produces perturbed upward drifts, favorable for ESF generation. Thus the Fejer-Scherliess model serves as a framework to establish the influence of geomagnetic storms on the generation or inhibition of equatorial irregularities.

[40] The example presented here, the 6 April 2000 storm, with a sharp increase in *AE* at ~1800 UT, showed irregularities in the East African sector, in accordance with the model's prediction that prompt penetration effects due to the magnetospheric dynamo would produce disturbance upward vertical drifts only in that postsunset period. From Table 1, additional case studies show that *AE* does not always experience sudden changes and other proxies, i.e., *dDst*/*dt*, are used to determine the penetration time. These case studies also show a consistent linkage between ESF onset and the behavior of the IMF B_z and IEF E_{sw}: equatorial ionospheric irregularities appear, after large and consistent southward excursions in the IMF B_z (enhanced E_{sw}) occur.

[41] Past studies have achieved a good level of success trying to identify the time when prompt penetration occurs at low latitudes. This has been possible without identification of the specific drivers of the index proxies used. To say that penetration occurs by following the behavior of a given index has thus served an important purpose, but it is now time to understand how this coupling between the different regions involved depends on specific physical mechanisms.

[42] **Acknowledgments.** This work was supported by the Office of Naval Research and the National Science Foundation. C.M. acknowledges the support of a CONICET Fellowship from Argentina. We thank the Center for Space Sciences at the University of Texas at Dallas and the US Air Force for providing the DMSP data. We thank the ACE MAG instrument team and the ACE Science Center for providing the ACE data. Finally, we acknowledge valuable discussions with Su. Basu, W. Burke, B. Fejer, L. Scherliess, and S. Sazykin.

[43] Arthur Richmond thanks the reviewers for their assistance in evaluating this paper.

References

Aarons, J. (1991), The role of the ring current in the generation or inhibition of equatorial F layer irregularities during magnetic storms, *Radio Sci.*, *4*, 1131.

Aarons, J. (1993), The longitudinal morphology of equatorial F layer irregularities relevant to their occurrence, *Space Sci. Rev.*, *63*, 209.

Aarons, J., et al. (1980), Seasonal and geomagnetic control of equatorial scintillations in two longitudinal sectors, *J. Atmos. Terr. Phys.*, *42*, 861.

Abdu, M. (1997), Major phenomena of the equatorial ionosphere-thermosphere system under disturbed conditions, *J. Atmos. Sol. Terr. Phys.*, *59*, 1505.

Ahn, B., S. Akasofu, and Y. Kamide (1983), The Joule heating production rate and the particle energy injection rate as a function of the geomagnetic indices AE and AL, *J. Geophys. Res.*, *88*, 6275.

Ahn, B., Y. Kamide, H. Krohel, and D. Gorney (1992), Cross-Polar cap potential difference, auroral electrojet indices, and solar wind parameters, *J. Geophys. Res.*, *97*, 1345.

Alex, S., and R. Rastogi (1986), Geomagnetic disturbance effect on equatorial spread-F, *Ann. Geophys.*, *5A*, 83.

Basu, Sa., et al. (2001), Response of the equatorial ionosphere in the South Atlantic region to the great magnetic storm of July 15, 2000, *Geophys. Res. Lett.*, *28*, 3577.

Basu, Su., et al. (2001), Ionospheric effects of major magnetic storms during the International Space Weather Period of September and October 1999: GPS observations, VHF/UHF scintillations, and in situ density structures at middle and equatorial latitudes, *J. Geophys. Res.*, *106*, 30,389.

Becker-Guedes, F., Y. Sahai, P. R. Fagundes, W. L. C. Lima, V. G. Pillat, R. Abalde, and J. A. Bittencourt (2004), Geomagnetic storm and equatorial spread-F, *Ann. Geophys.*, *22*, 3231.

Biktash, L. Z. (2004), Role of the magnetospheric and ionospheric currents in the generation of the equatorial scintillations during geomagnetic storms, *Ann. Geophys.*, *22*, 3195.

Blanc, M. (1978), Mid-latitude convection electric fields and their relation to ring current development, *Geophys. Res. Lett.*, *5*, 203.

Blanc, M., and A. Richmond (1980), The ionospheric disturbance dynamo, *J. Geophys. Res.*, *85*, 1669.

Boyle, C., P. Reiff, and M. Hairston (1997), Empirical polar cap potentials, *J. Geophys. Res.*, *102*, 111.

Burke, W., D. Weimer, and N. Maynard (1999), Geoeffective interplanetary scale sizes derived from regression analysis of polar cap potentials, *J. Geophys. Res.*, *104*, 9989.

Burton, R., R. McPherron, and C. Russel (1975), An empirical relationship between interplanetary conditions and Dst, *J. Geophys. Res.*, *80*, 4204.

Dabas, R., D. Laksmi, and B. Reddy (1989), Effect of geomagnetic disturbances on the VHF nighttime scintillation activity at equatorial and low latitudes, *Radio Sci.*, *24*, 563.

Farley, D., E. Bonelli, B. Fejer, and M. Larsen (1986), The prereversal enhancement of the zonal electric field in the equatorial ionosphere, *J. Geophys. Res.*, *91*, 13,723.

Fejer, B. (2002), Low latitude storm time ionospheric electrodynamics, *J. Atmos. Sol. Terr. Phys.*, *64*, 1401.

Fejer, B., and L. Scherliess (1997), Empirical model of storm-time equatorial zonal electric fields, *J. Geophys. Res.*, *102*, 24,047.

Fejer, B., C. Gonzales, D. Farley, M. Kelley, and R. Woodman (1979), Equatorial electric fields during magnetically disturbed conditions: 1. The effect of the interplanetary magnetic field, *J. Geophys. Res.*, *84*, 5797.

Fejer, B., L. Scherliess, and E. de Paula (1999), Effects of the vertical plasma drift velocity on the generation and evolution of equatorial spread F, *J. Geophys. Res.*, *104*, 19,859.

Fesen, C., G. Crowley, R. Roble, A. Richmond, and B. Fejer (2000), Simulation of the prereversal enhancement in the low latitude vertical ion drifts, *Geophys. Res. Lett.*, *27*, 1851.

Fuller-Rowell, T., G. Millward, A. Richmond, and M. Codrescu (2002), Storm-time changes in the upper atmosphere at low latitudes, *J. Atmos. Sol. Terr. Phys.*, *64*, 1383.

Gonzales, C., M. Kelley, B. Fejer, J. Vickrey, and R. Woodman (1979), Equatorial electric fields during magnetically disturbed conditions: 2. Implications of simultaneous auroral and equatorial measurements, *J. Geophys. Res.*, *84*, 5803.

Haerendel, G., and V. Eccles (1992), The role of the equatorial electrojet in the evening ionosphere, *J. Geophys. Res.*, *97*, 1181.

Haerendel, G., V. Eccles, and S. Çakir (1992), Theory for modeling the equatorial evening ionosphere and the origin of the shear in the horizontal plasma flow, *J. Geophys. Res.*, *97*, 1209.

Huang, C., W. Burke, J. Machuzak, L. Gentile, and P. Sultan (2001), DMSP observations of equatorial plasma bubbles in the topside ionosphere near solar maximum, *J. Geophys. Res.*, *106*, 8131.

Huang, C., W. Burke, J. Machuzak, L. Gentile, and P. Sultan (2002), Equatorial plasma bubbles observed by DMSP satellites during a full solar cycle: Toward a global climatology, *J. Geophys. Res.*, *107*(12), 1434, doi:10.1029/2002JA009452.

Jaggi, R., and R. Wolf (1973), Self-consistent calculation of the motion of a sheet of ions in the magnetosphere, *J. Geophys. Res.*, *78*, 2852.

Kelley, M., B. Fejer, and C. Gonzales (1979), Anomalous low latitude electric fields associated with a northward interplanetary magnetic field, *Geophys. Res. Lett.*, *6*, 301.

Kikuchi, T., H. Lühr, K. Schlegel, H. Tachihara, M. Shinohara, and T.-I. Kitamura (2000), Penetration of auroral electric fields to the equator during a substorm, *J. Geophys. Res.*, *105*, 23,251.

Lyon, A., N. Skinner, and R. Wright (1960), The belt of equatorial spread-F, *J. Atmos. Terr. Phys.*, *19*, 145.

Maruyama, T. (1988), A diagnostic model for equatorial spread F 1 Mode description and application to electric fields and neutral wind effects, *J. Geophys. Res.*, *93*, 14,611.

Maruyama, T., and N. Matuura (1984), Longitudinal variability of annual changes in activity of equatorial spread F and plasma bubbles, *J. Geophys. Res.*, *89*, 10,903.

Mendillo, M., B. Lin, and J. Aarons (2000), The application of GPS observations to equatorial aeronomy, *Radio Sci.*, *35*, 885.

Mendillo, M., J. Meriwether, and M. Biondi (2001), Testing the thermospheric neutral wind suppression mechanism for day-to-day variability of equatorial spread F, *J. Geophys. Res.*, *106*, 3655.

Nopper, R., and R. Carovillano (1978), Polar-equatorial coupling during magnetically active periods, *J. Geophys. Res.*, *83*, 699.

O'Brien, T., and R. McPherron (2000), An empirical phase space analysis of ring current dynamics: Solar wind control of injection and decay, *J. Geophys. Res.*, *105*, 7707.

Raghavarao, R., W. Hoegy, N. Spencer, and L. Wharton (1993), Neutral temperature anomaly in the equatorial thermosphere: A source of vertical winds, *Geophys. Res. Lett.*, *20*, 1023.

Rastogi, R., and V. Patel (1975), Effect of interplanetary magnetic field on ionosphere over the magnetic equator, *Proc. Indian Acad. Sci.*, *82*, 121.

Rastogi, R., J. Mullen, and E. MacKenzie (1981), Effect of geomagnetic activity on equatorial radio VHF scintillations and spread F, *J. Geophys. Res.*, *86*, 3661.

Reiff, P., and J. Luhmann (1986), Solar wind control of the polar-cap voltage, in *Solar Wind-Magnetosphere Coupling*, edited by Y. Kamide and J. A. Slavin, pp. 453–476, Terra Sci., Tokyo.

Richmond, A., C. Peymirat, and R. Roble (2003), Long-lasting disturbances in the equatorial ionospheric electric field simulated with a coupled magnetosphere-ionosphere-thermosphere model, *J. Geophys. Res.*, *108*(A3), 1118, doi:10.1029/2002JA009758.

Ridley, A., and M. Liemohn (2002), A model-derived storm time asymmetric ring current driven electric field description, *J. Geophys. Res.*, *107*(A8), 1151, doi:10.1029/2001JA000051.

Rothwell, P. L., J. R. Jasperse, W. Burke, N. Grossbard, and C. Huang (2004), Modeling the direct penetration of electric fields to the equatorial ionosphere, *Eos Trans. AGU*, *85*(17), Joint Assem. Suppl., Abstract SM33A-17.

Sahai, Y., P. Fagundes, J. Bittencourt, and M. Abdu (1998), Occurrence of large scale equatorial F-region plasma depletions during geo-magnetic disturbances, *J. Atmos. Sol. Terr. Phys.*, *60*, 1593.

Sahai, Y., P. Fagundes, J. Abalde, A. Pimenta, J. Bittencourt, Y. Otsuka, and V. Rios (2004), Generation of large-scale equatorial F-region plasma depletions during low range spread-F season, *Ann. Geophys.*, *22*, 15.

Sastri, J. (2002), Penetration electric fields at the nightside dip equator associated with the main impulse of the storm sudden commencement of 8 July 1991, *J. Geophys. Res.*, *107*(12), 1448, doi:10.1029/2002JA009453.

Sastri, J., M. Abdu, I. Batista, and J. Sobral (1997), Onset conditions of equatorial (range) spread *F* at Fortaleza, Brazil, during the June solstice, *J. Geophys. Res.*, *102*, 24,013.

Sazykin, S., R. Wolf, B. Fejer, R. Spiro, D. De Zeeuw, T. Gombosi, and J. Caldwell (2004), Ionospheric prompt penetration electric fields: Comparison of first-principle solutions with observations, *Eos Trans. AGU*, *84*(47), Fall Meeting Suppl., Abstract SM54A-03.

Scherliess, L., and B. Fejer (1997), Storm time dependence of equatorial disturbance dynamo zonal electric fields, *J. Geophys. Res.*, *102*, 24,037.

Senior, C., and M. Blanc (1984), On the control of magnetospheric convection by the spatial distribution of ionospheric conductivities, *J. Geophys. Res.*, *89*, 261.

Shen, C., Z. Liu, and T. Kamei (2002), A physics-based study of the *Dst-AL* relationship, *J. Geophys. Res.*, *107*(A1), 1009, doi:10.1029/2001JA900121.

Siscoe, G. (1982), Energy coupling between regions 1 and 2 Birkeland current systems, *J. Geophys. Res.*, *87*, 5124.

Siscoe, G., et al. (2002), Hill model of transpolar potential saturation: Comparisons with MHD simulations, *J. Geophys. Res.*, *107*(A6), 1075, doi:10.1029/2001JA000109.

Sobral, J., M. Abdu, H. Takahashi, M. Taylor, E. de Paula, C. Zamlutti, M. de Aquino, and G. Borba (2002), Ionospheric plasma bubble climatology over Brazil based on 22 years (1977–1998) of 630 nm airglow observations, *J. Atmos. Sol. Terr. Phys.*, *64*, 1517.

Southwood, D., and R. Wolf (1978), An assessment of the role of precipitation in magnetospheric convection, *J. Geophys. Res.*, *83*, 5227.

Stephan, A., M. Colerico, M. Mendillo, B. Reinisch, and D. Anderson (2002), Suppression of equatorial spread *F* by sporadic *E*, *J. Geophys. Res.*, *107*(A2), 1021, doi:10.1029/2001JA000162.

Sultan, P. (1996), Linear theory and modeling of the Rayleigh-Taylor instability leading to the occurrence of equatorial spread *F*, *J. Geophys. Res.*, *101*, 26,875.

Tsunoda, R. (1985), Control of the seasonal and longitudinal occurrence of equatorial scintillations by the longitudinal gradient in integrated *E* region Pederson conductivity, *J. Geophys. Res.*, *90*, 447.

Valladares, C. E., Jr., and R. E. Sheehan (2001), Measurement of the latitudinal distributions of total electron content during equatorial spread *F* events, *J. Geophys. Res.*, *106*, 29,133.

Wilson, G., W. Burke, N. Maynard, C. Huang, and H. Singer (2001), Global electrodynamics observed during the initial and main phases of the July 1991 magnetic storm, *J. Geophys. Res.*, *106*, 24,517.

J. Aarons, C. R. Martinis, and M. J. Mendillo, Center for Space Physics, Boston University, 725 Commonwealth Avenue, Boston, MA 02215, USA. (martinis@bu-ast.bu.edu)